

# Secondary-structure analysis of alcohol-denatured proteins by vacuum-ultraviolet circular dichroism spectroscopy

Koichi Matsuo,<sup>1</sup> Yoshie Sakurada,<sup>2</sup> Shin-ichi Tate,<sup>2</sup> Hirofumi Namatame,<sup>1</sup> Masaki Taniguchi,<sup>1</sup> and Kunihiro Gekko<sup>2\*</sup>

<sup>1</sup>Hiroshima Synchrotron Radiation Center, Hiroshima University, Higashi-Hiroshima 739-0046, Japan

<sup>2</sup>Department of Mathematical and Life Sciences, Graduate School of Science, Hiroshima University, Higashi-Hiroshima 739-8526, Japan

## ABSTRACT

To elucidate the structural characteristics of alcohol-denatured proteins, we measured the vacuum-ultraviolet circular dichroism (VUVCD) spectra of six proteins—myoglobin, human serum albumin,  $\alpha$ -lactalbumin, thioredoxin,  $\beta$ -lactoglobulin, and  $\alpha$ -chymotrypsinogen A—down to 170 nm in trifluoroethanol solutions (TFE: 0–50%) and down to 175 nm in methanol solutions (MeOH: 0–70%) at pH 2.0 and 25°C, using a synchrotron-radiation VUVCD spectrophotometer. The contents of  $\alpha$ -helices,  $\beta$ -strands, turns, poly-L-proline type II helices (PPIIs), and unordered structures of these proteins were estimated using the SELCON3 program, including the numbers of  $\alpha$ -helix and  $\beta$ -strand segments. Furthermore, the positions of  $\alpha$ -helices and  $\beta$ -strands on amino acid sequences were predicted by combining these secondary-structure data with a neural-network method. All alcohol-denatured proteins showed higher  $\alpha$ -helix contents (up to ~90%) compared with the native states, and they consisted of several long helical segments. The helix-forming ability was higher in TFE than in MeOH, whereas small amounts of  $\beta$ -strands without sheets were formed in the MeOH solution. The produced  $\alpha$ -helices were transformed dominantly from the  $\beta$ -strands and unordered structures, and slightly from the turns. The content and mean length of  $\alpha$ -helix segments decreased as the number of disulfide bonds in the proteins increased, suggesting that disulfide bonds suppress helix formation by alcohols. These results demonstrate that alcohol-denatured proteins constitute an ensemble of many long  $\alpha$ -helices, a few  $\beta$ -strands and PPIIs, turns, and unordered structures, depending on the types of proteins and alcohols involved.

Proteins 2012; 80:281–293.  
© 2011 Wiley Periodicals, Inc.

**Key words:** synchrotron-radiation circular dichroism; disulfide bond; methanol; trifluoroethanol; helix formation.

## INTRODUCTION

The structure of protein is stabilized with marginal energy and then easily denatured to various conformations by modification of the solvent conditions (e.g., type of organic solvent, temperature, pressure, and pH).<sup>1–3</sup> The structural characterization of denatured proteins is of fundamental importance for understanding the mechanisms of protein folding, stability, and amyloid formation.<sup>4–6</sup> Among various types of denaturation, alcohol denaturation is unique and has been extensively studied using many proteins and alcohols.<sup>7–10</sup> Alcohols disrupt the tertiary structure of a protein by exposing the internal hydrophobic residues to the solvent, but the denatured protein is rich in  $\alpha$ -helices, in contrast to other types of denaturation mainly disrupting  $\alpha$ -helices and producing considerable amounts of  $\beta$ -strands, turns, and poly-L-proline type II helices (PPIIs).<sup>11–14</sup> One conclusion of the recent studies is that the alcohol-denatured protein forms an open helical structure with strong local interactions within each helix but weak interactions between helical segments,<sup>15</sup> unlike the compact molten globule state stabilized by the interhelix hydrophobic inter-

Additional Supporting Information may be found in the online version of this article.  
*Abbreviations:* A-state, acid-denatured state; CD, circular dichroism; CGN,  $\alpha$ -chymotrypsinogen; FTIR, Fourier-transform infrared spectroscopy; HSA, human serum albumin; LA,  $\alpha$ -lactalbumin; LG,  $\beta$ -lactoglobulin; Mb, myoglobin; MeOH, methanol; NN, neural network; PPII, poly-L-proline type II helix; TFE, trifluoroethanol; Trx, thioredoxin; VUVCD, vacuum-ultraviolet circular dichroism.

Kunihiro Gekko's current address is Institute for Sustainable Sciences and Development, Hiroshima University, Higashi-Hiroshima 739-8526, Japan

Grant sponsor: JSPS Research Fellowship for Young Scientists (K.M.); Grant number: 19001913; Grant sponsor: Grant-in-Aid for Scientific Research from the Ministry of Education, Science, Sports, and Culture of Japan (K.G.); Grant number: 20550153

\*Correspondence to: Kunihiro Gekko, Department of Mathematical and Life Sciences, Graduate School of Science, Hiroshima University, Higashi-Hiroshima 739-8526, Japan. E-mail: gekko@hiroshima-u.ac.jp

Received 8 July 2011; Revised 7 September 2011; Accepted 19 September 2011  
Published online 26 September 2011 in Wiley Online Library (wileyonlinelibrary.com).  
DOI: 10.1002/prot.23206

actions.<sup>16,17</sup> However, although there is some evidence for the existence of  $\beta$ -strands,<sup>9,18,19</sup> the general features of the secondary structures (i.e., their contents, numbers of segments, and sequences) of alcohol-denatured proteins remain unclear because of the technical difficulties of studying highly fluctuating structures.

The structures of alcohol-denatured proteins have been studied using various techniques, including differential scanning calorimetry,<sup>20</sup> circular dichroism (CD),<sup>21,22</sup> nuclear magnetic resonance (NMR),<sup>4,23</sup> ultrasound,<sup>15</sup> mass spectrophotometry,<sup>8</sup> small-angle X-ray scattering,<sup>24,25</sup> and Fourier-transform infrared spectroscopy (FTIR).<sup>10</sup> NMR, FTIR, and CD can all be used to directly investigate the secondary structures, but CD spectroscopy is the most widely used because it is very sensitive to the local secondary structures and the CD spectra are measurable for any proteins at a low concentration under various solvent conditions. The secondary-structure analysis of proteins by CD spectroscopy has been markedly improved by (1) the development of programs (e.g., DSSP and Xtlstr) for assigning the secondary structures from atomic coordinates,<sup>26,27</sup> (2) advancements in the software (CONTIN, SELCON3, and CDSSTR) for analyzing the CD spectra,<sup>28,29</sup> and (3) the extension of CD measurements to the vacuum-ultraviolet region.<sup>30</sup> The short-wavelength limit of CD spectroscopy can be extended down to  $\sim 160$  nm by using synchrotron radiation as a high-flux source of photons, which yields much more information that cannot be obtained with a conventional CD spectrophotometer.<sup>31,32</sup> Thus, synchrotron-radiation vacuum-ultraviolet CD (VUVCD) spectroscopy is capable of estimating not only the contents but also the numbers of  $\alpha$ -helix and  $\beta$ -strand segments with high accuracy.<sup>33,34</sup> Furthermore, we have recently succeeded in improving the sequence-based prediction of secondary structures by combining VUVCD data with a neural-network (NN) algorithm (VUVCD-NN method).<sup>35–37</sup>

In this flux study, to elucidate the structural characteristics of alcohol-denatured proteins, we measured the VUVCD spectra of six proteins—myoglobin (Mb), human serum albumin (HSA),  $\alpha$ -lactalbumin (LA), thioredoxin (Trx),  $\beta$ -lactoglobulin (LG), and  $\alpha$ -chymotrypsinogen (CGN)—in trifluoroethanol (TFE) and methanol (MeOH) solutions. The secondary-structure contents of these proteins determined by X-ray analysis are listed in Table I together with the numbers of disulfide bonds. These proteins were examined because they encompass a wide variety of structures from  $\alpha$ - to  $\beta$ -types and their denaturation has been extensively investigated using various techniques.<sup>4,8,9,23,38,39</sup> TFE and MeOH were selected because they are among the alcohols having the strongest and weakest helix-inducing abilities, respectively, and hence are suitable for revealing the general denaturing effects of alcohols. The secondary structures (contents, numbers of segments, and sequences) of these alcohol-denatured proteins were compared with those of other denatured states<sup>14</sup> in order to generalize the structural characteristics of alcohol-denatured proteins.

**Table I**  
Structural Parameters of the Proteins Studied

Protein	PDB code	Content (%) <sup>a</sup> of			Number of disulfide bonds	Total residues
		$\alpha$ -helices	$\beta$ -strands	turns		
Mb	1WLA	73.8	0.0	13.1	0	153
HSA	1E78	69.9	0.0	14.9	17	585
LA	1F6S	30.9	8.1	20.3	4	123
Trx	2TRX	33.2	27.8	26.0	1	108
LG	1BEB	9.3	40.8	23.5	2	162
CGN	2CGA	7.4	32.2	20.4	5	245

<sup>a</sup>From crystal data listed in Protein Data Bank (PDB) code.

## MATERIALS AND METHODS

### Materials

Mb (from horse heart), HSA, LA (from bovine milk), Trx (from *Escherichia coli*), LG (from bovine milk), and CGN (from bovine pancreas) were purchased from Sigma (St. Louis, MO). These proteins were used without further purification. TFE and MeOH of high purity (>99.0%) were obtained from Sigma and Riedel-de Haën (Seelze, Germany), respectively. All other chemicals were analytical-grade products obtained from Sigma. The protein solutions dialyzed against double-distilled water at 4°C were adjusted to pH 2.0 with HCl to avoid aggregation with TFE and MeOH at various volume concentrations (10–50% and 10–70%, respectively). The final concentration of proteins was adjusted to 0.1% by absorption measurements (V-560, Jasco) with extinction coefficients of 17.9, 5.3, 11.4, and 9.6 dL g<sup>-1</sup> cm<sup>-1</sup> at 280 nm for Mb, HSA, Trx, and LG, respectively, and 20.1 dL g<sup>-1</sup> cm<sup>-1</sup> at 281.5 nm for LA, and 19.7 dL g<sup>-1</sup> cm<sup>-1</sup> at 282 nm for CGN.<sup>33,34</sup> The protein solutions obtained were centrifuged at 14,000 rpm for 15 min and then filtered by a membrane with a pore size of 20  $\mu$ m (DISMIC 25AS020AS, ADVANTEC) to remove the aggregates before CD measurements.

### CD measurements

The VUVCD spectra of proteins were measured from 260 to 170 nm for TFE solutions and down to 175 nm for MeOH solutions under a high vacuum (10<sup>-4</sup> Pa) using the VUVCD spectrophotometer constructed at Hiroshima Synchrotron Radiation Center and an assembled-type optical cell at 25°C.<sup>40,41</sup> The path length of the cell was adjusted with a Teflon spacer to 10  $\mu$ m. The details of the optical devices of the spectrophotometer and the optical cell are available elsewhere.<sup>41</sup> All of the VUVCD spectra were recorded with a 0.25-mm slit, a 16-s time constant, a 4-nm min<sup>-1</sup> scan speed, and 4–9 accumulations. The ellipticity was reproducible within an error of 5%, which was mainly attributable to noise and to inaccuracy in the optical path length.

## Secondary-structure analyses

The secondary structures of alcohol-denatured proteins were analyzed using the improved SELCON3 program<sup>28</sup> and the VUVCD spectra of the following 31 reference proteins with known X-ray structures<sup>33,34</sup> (their PDB codes are in parentheses): Mb (1WLA), hemoglobin (1G08), HSA (1E78), cytochrome *c* (1HRC), peroxidase (1ATJ), LA (1F6S), lysozyme (1HEL), ribonuclease A (1FS3), insulin (4INS), lactate dehydrogenase (9LDT), glucose isomerase (1OAD), lipase (3LIP), conalbumin (1OVT), transferrin (1LFG), catalase (7CAT), subtilisin A (1SBC),  $\alpha$ -amylase (1BAG), papain (9PAP), ovalbumin (1OVA), LG (1BEB), pepsin (4PEP), trypsinogen (1TGN), CGN (2CGA), soybean trypsin inhibitor (1AVU), concanavalin A (2CTV), staphylococcal nuclease (1EY0), Trx (2TRX), carbonic anhydrase (1G6V), elastase (3EST), avidin (1AVE), and xylanase (1ENX). The secondary structures of these proteins in crystal form were assigned using the DSSP program<sup>26</sup> based on the numbers and positions of hydrogen bonds between peptide groups. The bends were treated as turns, and the single residues assigned as turns and bends were classified as unordered structures. Moreover,  $\alpha$ -helices and  $\beta$ -strands were divided into regular ( $\alpha_R$  and  $\beta_R$ ) and distorted ( $\alpha_D$  and  $\beta_D$ ) classes, assuming that four residues per  $\alpha$ -helix and two residues per  $\beta$ -strand were distorted.<sup>29</sup> This classification resulted in the protein structures being classified into six types: regular  $\alpha$ -helix ( $\alpha_R$ ), distorted  $\alpha$ -helix ( $\alpha_D$ ), regular  $\beta$ -strand ( $\beta_R$ ), distorted  $\beta$ -strand ( $\beta_D$ ), turn, and unordered structure. The contents of these secondary structures were estimated using the SELCON3 program, and the numbers of  $\alpha$ -helix and  $\beta$ -strand segments were calculated from the  $\alpha_D$  and  $\beta_D$  contents, respectively.<sup>29</sup> The content of PPII, which is grouped as an unordered structure in the DSSP program, was also estimated using the SELCON3 and Xtlstr programs<sup>27</sup> for further comparison of the alcohol-denatured structures with the cold-, heat-, and acid-denatured ones previously elucidated by VUVCD spectroscopy.<sup>14</sup>

## Sequence-based prediction of secondary structures

The positions of secondary structures ( $\alpha$ -helices and  $\beta$ -strands) on the amino acid sequence were predicted by the VUVCD-NN method.<sup>35</sup> We adopted the NN algorithm developed by Jones,<sup>42</sup> which predicts the position of secondary structures using the evolutionary sequence information based on the position-specific scoring matrices generated by the PSI-BLAST algorithm. A training data set of 607 proteins was prepared from the X-ray structures in the PDB (September 2006 version)<sup>43</sup> by eliminating the short chains (<30 residues), unidentified sequences, similar sequences (>25%), and chain breaks.<sup>35</sup> The weights and biases of 20 amino acids for  $\alpha$ -helices and  $\beta$ -strands were calculated from the second-

ary structures and amino acid sequences of these 607 proteins using a freeware simulation package (Stuttgart Neural Network Simulator, version 4.2).<sup>44</sup>

The positions of  $\alpha$ -helices and  $\beta$ -strands on the amino acid sequence were assigned in descending order of the  $\alpha$ -helix and  $\beta$ -strand weights of the 20 amino acids until the determined numbers of  $\alpha$ -helix and  $\beta$ -strand residues converged to those estimated from the VUVCD analysis. Next, the numbers of  $\alpha$ -helix and  $\beta$ -strand segments estimated from the VUVCD analysis were introduced into the NN calculation until the predicted numbers of segments converged to those obtained from the VUVCD estimation. If the predicted numbers of residues and segments for  $\alpha$ -helices and  $\beta$ -strands did not converge to the VUVCD estimates, the sequence alignment that minimized the difference between the two estimates was taken as the final solution. The predictive accuracy of this VUVCD-NN method was 75% for 30 of the 31 reference proteins (the exception being insulin). The computational protocol for the VUVCD-NN method was detailed previously.<sup>35</sup>

## RESULTS

### VUVCD spectra of alcohol-denatured proteins

The VUVCD spectra of six proteins (Mb, HSA, LA, Trx, LG, and CGN) were successfully measured down to 170 nm in the TFE solutions (0–50%) and down to 175 nm in the MeOH solutions (0–70%) at pH 2.0 and 25°C (Fig. 1). These spectra were constant during the data-acquisition period (about 2 h) under all solvent conditions, indicating that the synchrotron radiation (0.7 GeV) did not damage the protein structure. The molar ellipticities at 222 and 192 nm are plotted against the TFE and MeOH concentrations in the inset of each graph.

Mb exhibited a typical acid-denatured spectrum at pH 2.0. This spectrum changed cooperatively into  $\alpha$ -helix-type spectra by the addition of TFE, with almost saturating behavior at 50% TFE [Fig. 1(a)], as observed by conventional CD spectroscopy.<sup>21</sup> Interestingly, the CD intensities at 222, 208, and 192 nm were larger in 50% TFE than in the native state, suggesting that the amount of  $\alpha$ -helices was significantly increased in 50% TFE. Compared with TFE, MeOH at 70% showed a less cooperative transition and no saturation [Fig. 1(b)] although apoMb showed the same intensity at 222 nm in both 80% TFE and 80% MeOH solutions.<sup>21</sup> These results suggest that the secondary structures of Mb differ in 50% TFE and 70% MeOH. HSA and LA also exhibited  $\alpha$ -helix-type spectra with isoellipticity points around 202 and 175 nm in the TFE and MeOH solutions [Fig. 1(c–f)], with the spectra in the far-UV region being similar to those observed by conventional CD spectroscopy.<sup>45,46</sup>

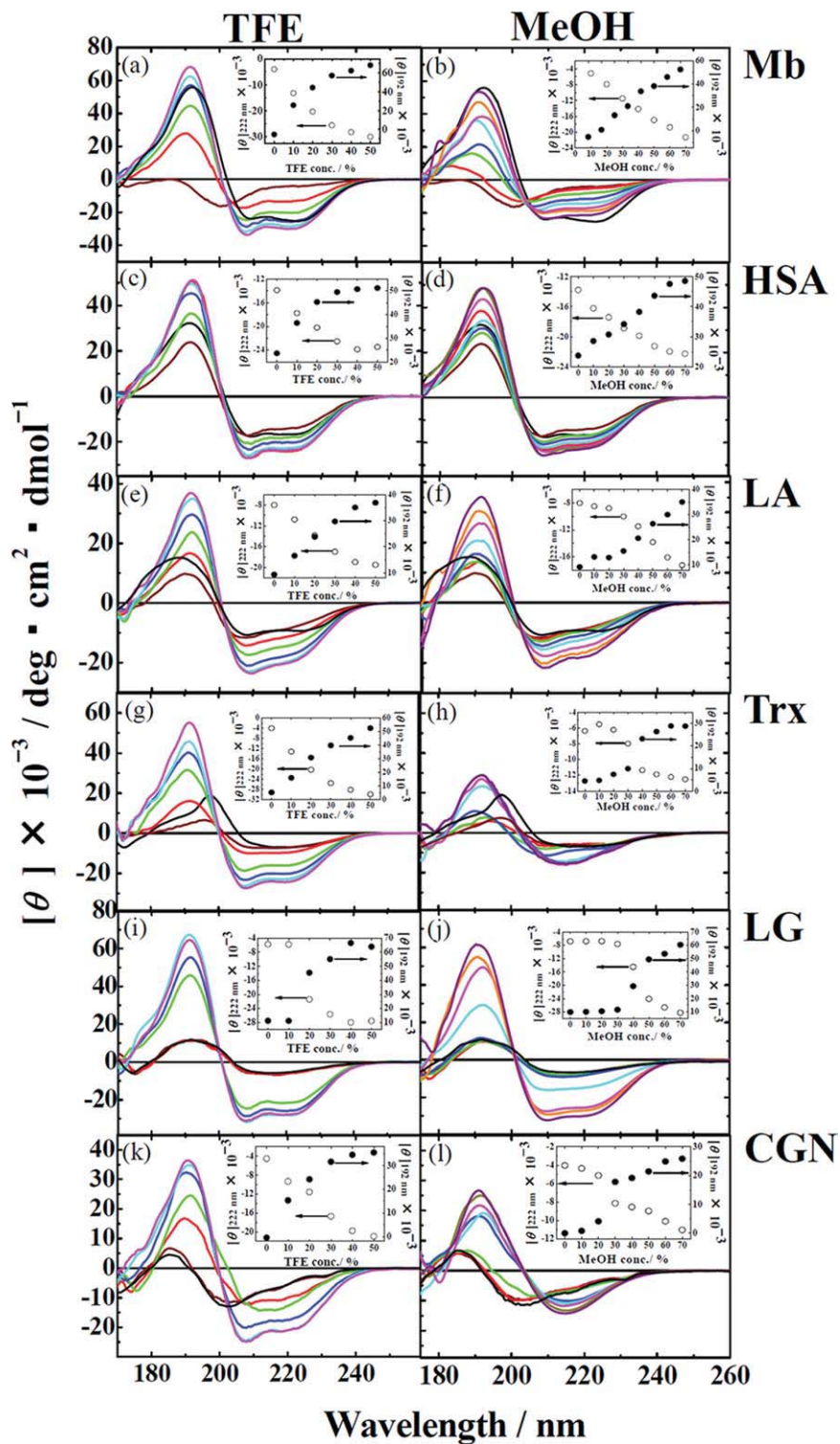


**Figure 1**

VUVCD spectra of alcohol-denatured proteins at pH 2.0 and 25°C. Panels from top to bottom represent Mb, HSA, LA, Trx, LG, and CGN, respectively, in the TFE (left panels) and MeOH (right panels) solutions. Colored spectra refer to the native state (black), A-state (brown), and alcohol concentrations of 10% (red), 20% (green), 30% (dark blue), 40% (light blue), 50% (pink), 60% (orange), and 70% (violet). Insets show plots of the molar ellipticities at 222 nm (open circles) and 192 nm (solid circles) (left and right vertical axes, respectively) against the TFE and MeOH concentrations.

**Table II**

Secondary-Structure Contents and Numbers of Segments of Mb, HSA, La, Trx, LG, and CGN in the Native, Acid-, TFE-Denatured, and MeOH-Denatured States as Determined by VUVCD Spectroscopy

State <sup>a</sup>	$\alpha$ -Helices		$\beta$ -Strands		Turns (%)	Unordered structures (%)	PPII (%) <sup>c</sup>
	Content (%)	Number <sup>b</sup>	Content (%)	Number <sup>b</sup>			
<b>Mb</b>							
Native (X-ray)	73.8	8 (14)	0.0	0	13.1	13.1	1.3
Native (pH 5.4, 25°C)	71.5 $\pm$ 0.9	8 (14)	-1.2 $\pm$ 0.6	0	15.4 $\pm$ 0.1	9.4 $\pm$ 0.5	1.2 $\pm$ 0.1
Acid-denatured	4.8 $\pm$ 1.0	2 (4)	27.2 $\pm$ 2.0	9 (5)	21.4 $\pm$ 1.0	49.6 $\pm$ 1.8	16.4 $\pm$ 0.6
TFE-denatured	93.3 $\pm$ 1.3	7 (20)	-2.7 $\pm$ 0.5	0	11.4 $\pm$ 0.4	2.0 $\pm$ 0.6	0.3 $\pm$ 0.1
MeOH-denatured	73.1 $\pm$ 0.5	6 (19)	3.3 $\pm$ 1.7	1 (5)	20.6 $\pm$ 0.9	5.3 $\pm$ 1.7	-1.0 $\pm$ 0.1
<b>HSA</b>							
Native (X-ray)	69.6	29 (14)	0.0	0	14.9	15.5	3.8
Native (pH 5.0, 25°C)	58.6 $\pm$ 0.8	31 (11)	-2.2 $\pm$ 2.2	0	19.5 $\pm$ 1.0	27.1 $\pm$ 1.5	2.5 $\pm$ 0.7
Acid-denatured	47.4 $\pm$ 4.6	26 (11)	4.4 $\pm$ 2.2	9 (3)	16.4 $\pm$ 0.6	34.3 $\pm$ 0.4	6.5 $\pm$ 0.6
TFE-denatured	83.6 $\pm$ 1.4	32 (15)	-1.2 $\pm$ 0.8	0	15.1 $\pm$ 2.0	9.7 $\pm$ 0.1	1.8 $\pm$ 2.0
MeOH-denatured	76.8 $\pm$ 3.9	31 (14)	-0.9 $\pm$ 0.8	0	13.9 $\pm$ 0.3	12.5 $\pm$ 3.0	3.5 $\pm$ 0.3
<b>LA</b>							
Native (X-ray)	30.9	4 (10)	8.1	3 (3)	20.3	40.7	1.5
Native (pH 7.3, 25°C)	31.8 $\pm$ 1.8	4 (10)	16.1 $\pm$ 2.4	4 (5)	20.1 $\pm$ 0.8	31.1 $\pm$ 1.6	7.0 $\pm$ 0.8
Acid-denatured	20.2 $\pm$ 0.9	5 (5)	18.3 $\pm$ 1.5	5 (5)	21.9 $\pm$ 0.9	30.7 $\pm$ 3.0	8.4 $\pm$ 1.0
TFE-denatured	69.8 $\pm$ 3.6	7 (12)	-0.3 $\pm$ 4.2	0	16.0 $\pm$ 0.9	16.8 $\pm$ 1.0	3.2 $\pm$ 0.1
MeOH-denatured	68.7 $\pm$ 0.2	7 (12)	5.1 $\pm$ 0.3	1 (6)	15.7 $\pm$ 0.1	16.7 $\pm$ 0.6	3.1 $\pm$ 0.1
<b>Trx</b>							
Native (X-ray)	33.2	4 (9)	27.8	5 (6)	26.0	13.0	4.2
Native (pH 5.8, 25°C)	32.8 $\pm$ 1.2	5 (7)	23.5 $\pm$ 0.5	4 (6)	24.1 $\pm$ 1.4	20.0 $\pm$ 1.6	4.3 $\pm$ 1.1
Acid-denatured	20.4 $\pm$ 3.2	3 (7)	23.7 $\pm$ 3.8	5 (5)	21.1 $\pm$ 1.8	32.0 $\pm$ 1.3	8.0 $\pm$ 0.8
TFE-denatured	87.1 $\pm$ 0.8	6 (16)	-3.2 $\pm$ 0.7	0	15.4 $\pm$ 1.5	5.7 $\pm$ 2.0	0.4 $\pm$ 0.1
MeOH-denatured	45.5 $\pm$ 0.7	4 (12)	12.8 $\pm$ 1.4	2 (7)	18.7 $\pm$ 1.5	25.1 $\pm$ 1.1	5.2 $\pm$ 0.4
<b>LG</b>							
Native (X-ray)	9.3	2 (8)	40.8	10 (7)	23.5	26.5	4.5
Native (pH 6.6, 25°C)	11.5 $\pm$ 1.7	2 (9)	37.2 $\pm$ 4.6	9 (7)	25.2 $\pm$ 1.2	28.7 $\pm$ 1.7	6.7 $\pm$ 0.6
Acid-denatured	14.0 $\pm$ 2.0	2 (11)	36.5 $\pm$ 4.2	9 (7)	17.5 $\pm$ 0.9	31.8 $\pm$ 0.5	6.8 $\pm$ 0.1
TFE-denatured	88.2 $\pm$ 0.6	9 (16)	-3.7 $\pm$ 2.2	0	9.8 $\pm$ 0.5	5.3 $\pm$ 2.4	1.7 $\pm$ 0.9
MeOH-denatured	83.9 $\pm$ 0.3	9 (15)	0.6 $\pm$ 0.6	0	13.5 $\pm$ 0.4	3.7 $\pm$ 0.3	2.3 $\pm$ 0.6
<b>CGN</b>							
Native (X-ray)	7.4	2 (9)	32.2	14 (6)	20.4	40.0	11.5
Native (pH 5.6, 25°C)	8.1 $\pm$ 0.8	3 (7)	29.7 $\pm$ 3.1	15 (5)	21.6 $\pm$ 1.2	39.9 $\pm$ 1.9	12.5 $\pm$ 1.0
Acid-denatured	12.1 $\pm$ 0.7	3 (10)	23.9 $\pm$ 1.6	13 (5)	20.7 $\pm$ 0.8	40.8 $\pm$ 0.7	8.9 $\pm$ 0.1
TFE-denatured	63.7 $\pm$ 0.7	12 (13)	5.1 $\pm$ 2.1	3 (4)	15.0 $\pm$ 0.1	20.2 $\pm$ 1.3	4.3 $\pm$ 0.1
MeOH-denatured	40.2 $\pm$ 0.7	10 (10)	14.3 $\pm$ 1.3	7 (5)	16.4 $\pm$ 1.7	27.6 $\pm$ 2.5	6.1 $\pm$ 0.7

<sup>a</sup>Acid-, TFE-, and MeOH-denatured states measured at pH 2.0 and 25°C.<sup>b</sup>Values in parentheses are the mean numbers of residues per  $\alpha$ -helix or  $\beta$ -strand.<sup>c</sup>Assigned by Xtlsstr method.

The transition curves for both proteins were almost saturated in 50% TFE and 70% MeOH, but LA appeared to be not completely denatured in 70% MeOH. On the other hand, Trx, which contains comparable amounts of  $\alpha$ -helices and  $\beta$ -strands (Table I), exhibited significantly different spectra in the TFE and MeOH solutions [Fig. 1(g,h)]. TFE induced the typical  $\alpha$ -helix-type spectrum, with almost complete saturation in 50% TFE, whereas MeOH induced the  $\beta$ -strand-type spectrum in a highly cooperative manner, with saturation induced by 70% MeOH, suggesting the complicated alcohol denaturation of Trx.

LG showed the  $\beta$ -strand-type spectrum at both pH 2.0 and neutral pH (native state), with a positive peak around 192 nm and two negative peaks around 215 and 175 nm [Fig. 1(i,j)]. This spectrum was cooperatively transformed into the  $\alpha$ -helix-type spectrum with isoellipticity points around 202 and 175 nm in the TFE and MeOH solutions,

as observed for Mb, HSA, and LA. CGN also showed the  $\beta$ -strand-type spectrum at pH 2.0 as well as at neutral pH (native state), with a positive peak around 185 nm, a negative peak around 205 nm, and a shoulder around 220–230 nm [Fig. 1(k,l)]. However, different from LG, this spectrum was transformed into the  $\alpha$ -helix type via a  $\beta$ -strand spectrum in 30% TFE, as demonstrated by a negative peak around 215 nm. The MeOH-induced spectra were also different from the  $\alpha$ -helix-type, suggesting the presence of a considerable amount of  $\beta$ -strands in both the MeOH-denatured CGN and Trx.

### Secondary structures of alcohol-denatured proteins

As shown in Figure 1, extending the short-wavelength limit of CD spectra yields much more information on

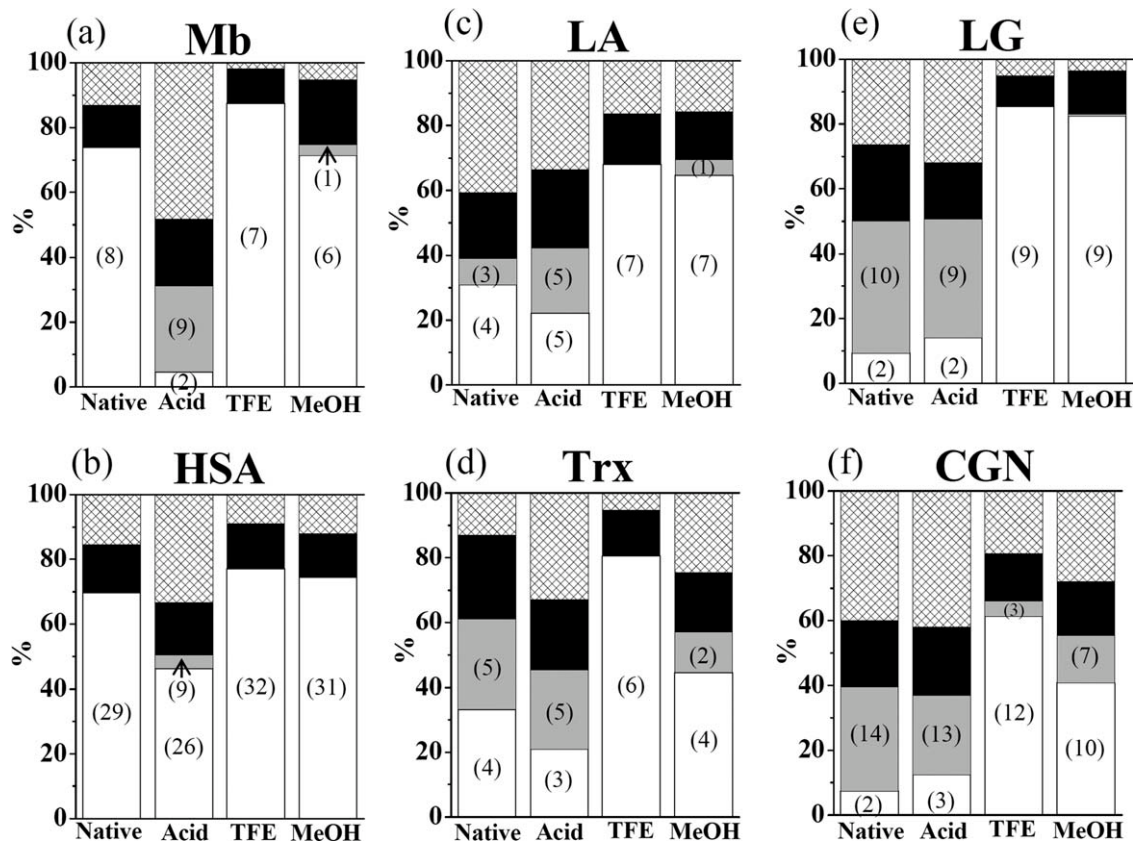


**Figure 2**

Histograms of the secondary-structure contents of native, acid-, TFE-, and MeOH-denatured Mb (a), HSA (b), LA (c), Trx (d), LG (e), and CGN (f). The structures shown are  $\alpha$ -helices (white rectangles),  $\beta$ -strands (gray rectangles), turns (black rectangles), and unordered structures (hatched rectangles). The values in parentheses attached to each rectangle indicate the numbers of  $\alpha$ -helix and  $\beta$ -strand segments (see Table II).

the secondary structures compared with conventional CD spectroscopy and increases the accuracy of estimates of the contents and numbers of  $\alpha$ -helix and  $\beta$ -strand segments of the alcohol-denatured proteins. The root-mean-square deviation ( $\delta$ ) and the Pearson correlation coefficient ( $r$ ) between the X-ray and VUVCD estimates of the secondary-structure contents for 31 reference proteins were 0.058 and 0.92, respectively, demonstrating the high accuracy of the VUVCD estimation.<sup>34</sup>

The estimated secondary-structure contents of six proteins in 50% TFE and 70% MeOH are listed in Table II, together with those in the native state and in the acid-denatured (pH 2.0) state (A-state). For ease of comparison, the results in Table II are depicted as histograms in Figure 2, with the secondary-structure contents normalized to a total content of 100%, and the histogram for the native state depicted with the results obtained from the DSSP program.

The numbers of  $\alpha$ -helix and  $\beta$ -strand segments have been estimated from the CD spectra using two methods: (1) Pancoska et al.<sup>47</sup> used a matrix descriptor of secondary-structure segments for the NN-based analysis of pro-

teins and (2) Sreerama et al.<sup>29</sup> estimated the numbers of segments from the distorted residues of  $\alpha$ -helices and  $\beta$ -strands, assuming that on average there were four and two distorted residues per  $\alpha$ -helix and  $\beta$ -strand, respectively. The results of these two analyses are comparable, and hence we used the method of Sreerama et al.<sup>29</sup> The estimated numbers of  $\alpha$ -helix and  $\beta$ -strand segments are listed in Table II and Figure 2.

We also estimated the content of the PPII structure, which is a left-handed three-fold helix,<sup>13</sup> because there were considerable amounts of the short PPII stretches in the cold- and heat-denatured states, A-state, and urea- and guanidine-hydrochloride-unfolded states.<sup>14</sup> The  $\delta$  and  $r$  between the X-ray and VUVCD estimates of the PPII contents for 31 reference proteins were 0.053 and 0.71, respectively. Although both values are smaller than those for  $\alpha$ -helix and  $\beta$ -strand,<sup>34,35</sup> the PPII contents of six proteins were estimated within a few percent except for LA as indicated in Table II. Evidently, the proteins in 50% TFE and 70% MeOH had a smaller PPII content (less than 6%, average 2.3%) compared with proteins denatured by other means (average

13.8%),<sup>14</sup> indicating that PPII is hardly formed in alcohol-denatured proteins.

### Predicted sequences of secondary structures

CD spectroscopy itself in principle yields no information on the sequences of the secondary structures, and hence an algorithm exploiting the correlations between the X-ray structures and amino acid sequences of many proteins is necessary for the sequence-based prediction of secondary structures such as  $\alpha$ -helices and  $\beta$ -strands. In this study, we used the NN algorithm of Jones<sup>42</sup> due to the technical convenience of combining it with VUVCD data. In this analysis, the weights of 20 amino acids were calculated without considering the solvent dependence, because the intrinsic solvent dependence is generally difficult to evaluate. However, the effects of the solvent on the weights would introduce only small errors into sequence prediction by the VUVCD-NN method because VUVCD spectroscopy can predict the contents and numbers of secondary-structure segments much more accurately than can NN analysis.<sup>35</sup> Therefore, the VUVCD-NN method will be valuable for predicting the sequences of secondary structures in alcohol-denatured proteins. In the predictions performed in this study, the turns and unordered structures estimated using the SELCON3 program were classified into "others."

The positions of  $\alpha$ -helices,  $\beta$ -strands, and others predicted for Mb, Trx, and CGN in the native, A- (pH 2.0), TFE- (50% TFE), and MeOH-denatured (70% MeOH) states are depicted on the amino acid sequence in Figure 3, which also includes those determined from X-ray data for comparison. The secondary-structure sequences predicted for HSA, LA, and LG are given in Figure S1 (Supporting Information). The prediction accuracies of these sequences were 83.7%, 79.6%, 71.8%, 76.6%, 55.3%, and 72.2% for Mb, Trx, CGN, HSA, LA, and LG, respectively, in terms of the success rate (quantified as the  $Q_3$  value) between the X-ray and VUVCD-NN estimates for the native structure. Most of the alcohol-denatured proteins consisted of several long  $\alpha$ -helices and very few (or no)  $\beta$ -strands, whereas the MeOH-denatured Trx and CGN contained several  $\beta$ -strands in addition to  $\alpha$ -helices. The numbers of segments predicted at the sequence level did not necessarily agree with those predicted from VUVCD data because sequence-alignment minimization was performed in the VUVCD-NN method (see Materials and Methods).

## DISCUSSION

The present VUVCD study produced much more detailed information about the secondary structures of alcohol-denatured proteins than does conventional CD spectroscopy, and has for the first time predicted the

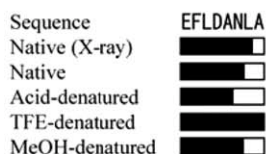
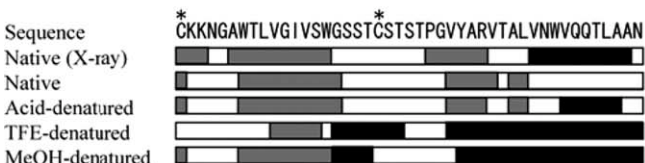
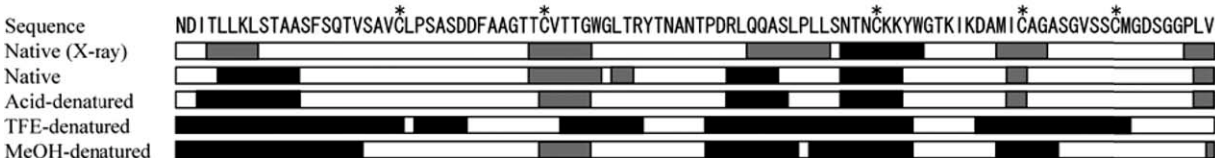
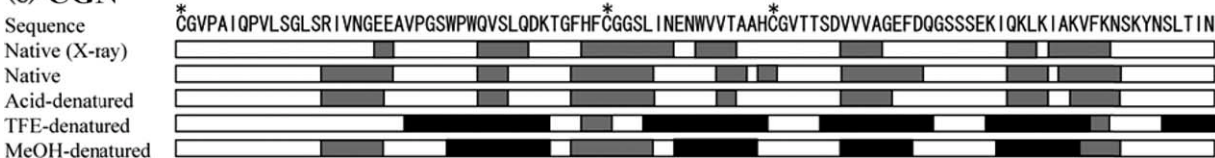
numbers and sequences of  $\alpha$ -helix and  $\beta$ -strand segments. The newly obtained information is very useful for characterizing the secondary structures of alcohol-denatured proteins in comparison with the native state and other types of denatured states. The analytical results for individual proteins should be discussed first for deriving the general features of protein structures in alcohol solutions.

### Structures of alcohol-denatured proteins

*Myoglobin*—Alcohol denaturation of Mb has been widely investigated using various techniques such as NMR, FTIR, mass spectrometry, and CD spectroscopy.<sup>8,21,24</sup> Mb is a simple monomeric protein without disulfide bonds or  $\beta$ -strands, but its alcohol-denatured state remains undefined, as is also the case for many other proteins. Before addressing the alcohol-denatured state, it is pertinent to briefly discuss the structure of the A-state, which is a reference state for alcohol denaturation.

As indicated in Table II and Figure 2(a), the A-state of Mb comprises 4.8%  $\alpha$ -helices (two segments), which is much less than the 73.8% (eight segments) present in the native state. These contents, numbers of segments, and the predicted sequences of  $\alpha$ -helices (Fig. 3) are consistent with the results of two-dimensional NMR<sup>48</sup> indicating that parts of the A-helix (residues 4–18) and H-helix (residues 125–149) are preserved in the A-state of apoMb (pH 2.3). However, our VUVCD analysis predicted 27.2%  $\beta$ -strands consisting of nine segments, although no evidence for their presence was obtained in the NMR experiments, probably because the fluctuations of the denatured protein are much faster than the detection time of signals associated with the Nuclear Overhauser Effect of NMR. These results suggest that  $\beta$ -strands in the A-state do not exist as  $\beta$ -sheets but rather as an ensemble of numerous short peptide segments with the dihedral angles of a  $\beta$ -strand.<sup>16</sup>

The VUVCD spectra clearly reveal that adding TFE and MeOH induces helix-rich structures [Fig. 1(a,b)]. The conformational changes seem to be essentially a two-state transition, as judged from the ellipticity plots at 222 and 192 nm, and the isoellipticity points at 202 and 175 nm. However, some shoulders in the transition curve for 30–40% MeOH [inset of Fig. 1(b)] suggest the existence of intermediate structures during MeOH denaturation, which were detected by NMR<sup>24</sup> and H/D exchange monitored by mass spectrometry.<sup>8</sup> Although the transition curves do not appear to saturate, the structures of Mb in 50% TFE and 70% MeOH would be close to those that are completely denatured by the respective alcohols. As indicated in Table II and Figure 2(a), TFE and MeOH induce significant amounts of  $\alpha$ -helices (93.3% and 73.1%, respectively) and negligible amounts of  $\beta$ -strands, which are similar to the results of a conventional CD investigation of apoMb in 80% TFE and 80% MeOH at

**(a) Mb****(b) Trx****(c) CGN****Figure 3**

Sequence-based secondary structures of alcohol-denatured Mb (a), Trx (b), and CGN (c) predicted by the VUVCD-NN method. The  $\alpha$ -helices,  $\beta$ -strands, and coil structures are shown in black, gray, and white, respectively. The secondary-structure regions of the wild type were assigned using the DSSP program from the X-ray structure. The cysteine residues taking part in disulfide bonds are marked with asterisks (\*). The predicted sequences for HSA, LA, and LG are shown in Figure S1 (Supporting Information).

pH 2.0.<sup>21</sup> Evidently, the increased helices are transformed from the coil, turn, and  $\beta$ -strand regions of the acid-denatured structure [Fig. 2(a)]. The  $\alpha$ -helices induced by TFE and MeOH comprised seven segments (with 20 residues) and six segments (with 19 residues) on average,

respectively, compared with eight segments (with mean 14 residues) in the  $\alpha$ -helices in the native structure. These findings suggest that the  $\alpha$ -helices in alcohol-induced proteins are considerably longer than those in the native structures.

It is of interest to estimate the positions of  $\alpha$ -helix and  $\beta$ -strand segments on the amino acid sequences of denatured proteins. Figure 3(a) shows the sequences of secondary structures of Mb predicted by the VUVCD-NN method in the native, A-, TFE-, and MeOH-denatured states. Although the VUVCD-NN method—which is based on the standards of the native structure—may have limited applicability to the denatured proteins, we can deduce certain characteristic features of alcohol-denatured states from the sequence-based prediction because this method has a high prediction accuracy for this protein ( $Q_3 = 83.7\%$ ). Most of the coil (turn plus unordered) and  $\beta$ -strand regions in the A-state are transformed into  $\alpha$ -helices in the TFE and MeOH solutions, lengthening the two helices present in the A-state. There are only minor differences in the sequences of the structures induced by TFE and MeOH, with some coil and  $\beta$ -strand residues in the MeOH solution being replaced by helices in the TFE solution. It is noteworthy that most coil regions between adjacent  $\alpha$ -helices present in the native state are preserved in the A- and alcohol-denatured states, whereas two coil residues between A-helix (residues 4–18) and B-helix (residues 21–35) and six coil residues between E-helix (residues 59–76) and F-helix (residues 83–95) are transformed into  $\alpha$ -helices, joining the two adjacent helices to a single long helix. These results suggest that there is no marked difference in the arrangement of  $\alpha$ -helices between the native and alcohol-denatured states, although the tertiary structure is disrupted in the alcohol solutions.

*Human serum albumin*—HSA is a helix-rich protein (69.6%) consisting of 29 helix segments and three domains with 17 disulfide bonds.<sup>49</sup> As indicated in Table II and Figure 2(b), the content and number of  $\alpha$ -helix segments decrease to 47.4% and 26, respectively, in the A-state (pH 2.0), but increase to 83.6% and 32 (with mean 15 residues) in 50% TFE, and to 76.8% and 31 (with mean 16 residues) in 70% MeOH. These results indicate that the two alcohols induce very similar secondary structures of this protein, as suggested in a previous study.<sup>38</sup> This similarity in the secondary structures can also be found in the amino acid sequences predicted by the VUVCD-NN method (Supporting Information Fig. S1). As in the case of Mb, most coil regions connecting the adjacent helices in the native state are preserved in the alcohol-denatured states, but TFE might exert a higher helix-forming ability than MeOH for some coil regions such as residues 223–227, 362–365, and 371–373. Evidently, many helices induced by both alcohols maintain a longer average length than those in the native structure.

*$\alpha$ -Lactalbumin*—LA is an  $\alpha/\beta$ -type protein with four disulfide bonds consisting of four  $\alpha$ -helices (30.9%) and three  $\beta$ -strands (8.1%). In the A-state of LA, which is known as the partially folded molten globule state,<sup>50</sup> the helix content decreases to 20.2% but its number of

segments increases to five, whereas the content and number of  $\beta$ -strand segments increase to 18.3% and five, respectively [Table II and Fig. 2(c)]. Evidently, TFE and MeOH induce helix-rich structures (about 70% and seven segments), although a small amount of  $\beta$ -strands may be produced in the MeOH solution (Table II).

The secondary-structure sequences of LA predicted by the VUVCD-NN method are given in Figure S1 (Supporting Information). Although the prediction accuracy is low for this protein ( $Q_3 = 55.3\%$ ), it is assumed that four  $\alpha$ -helices present in the native state are preserved or extended, several coil and  $\beta$ -strand regions change into  $\alpha$ -helices, and a long  $\alpha$ -helix is formed in the C-terminal region. NMR provides corroborative evidence for these conformational changes: the content and number of helix segments in guinea pig LA—whose tertiary structure is very similar to that of bovine LA—increase in the TFE solution, and the newly formed  $\alpha$ -helices are mainly localized in the coil regions of the native structure.<sup>4</sup>

*Thioredoxin*—Trx is an  $\alpha/\beta$ -type protein (comprising 33.2%  $\alpha$ -helices, 27.8%  $\beta$ -strands, 26.0% turns, and 13.0% unordered structures) with one disulfide bond comprising a five-stranded twisted  $\beta$ -sheet surrounded by four  $\alpha$ -helices. As indicated in Table II and Figure 2(d), the  $\alpha$ -helix content decreases to 20.4% and the unordered-structure content increases to 32.2% in the A-state, suggesting that the dominant conformational change in the acid denaturation is a transition from helices to unordered structures. There are large differences in the secondary structures induced by TFE and MeOH: TFE induces 87.1%  $\alpha$ -helices with mean 16 residues and no  $\beta$ -strands, whereas MeOH exhibits no such strong helix-forming ability (45.5% helices with mean 12 residues) and induces 12.8%  $\beta$ -strands. Furthermore, an isoelliptic point near 205 nm in the VUVCD spectra [Fig. 1(h)] at higher MeOH concentrations suggests the formation of intermediates during MeOH denaturation. These structural differences are also identified in the secondary-structure sequences predicted by the VUVCD-NN method ( $Q_3 = 79.6\%$ ; Fig. 3). Four  $\alpha$ -helices present in the native state, one of which (residues 66–69) is broken in the A-state, are extended in the TFE and MeOH solutions, with a longer average length for TFE. Three of five  $\beta$ -strands in the native state are changed into  $\alpha$ -helices or coils, but two  $\beta$ -strands (residues 22–28 and 53–59) forming an antiparallel sheet in the native state appear to be preserved in the MeOH solution.

*$\beta$ -Lactoglobulin*—LG is a  $\beta$ -strand-rich protein (comprising 40.8%  $\beta$ -strands and 9.3%  $\alpha$ -helices) with two disulfide bonds, and it forms a dimer in aqueous solution. As expected from the similar CD spectra [Fig. 1(i)], there is no clear difference in the contents and numbers of  $\beta$ -strand and  $\alpha$ -helix segments between the native and A-states (Table II and Fig. 3), which is consistent with the NMR data indicating that LG maintains a native-like structure and dissociates into monomer at pH 2.0.<sup>23,51</sup>

In both TFE and MeOH solutions, all  $\beta$ -strands disappear and about 85%  $\alpha$ -helices (nine segments of mean 15 residues) are produced. The numbers of  $\alpha$ -helix segments predicted by the VUVCD-NN method (Supporting Information Fig. S1) differ considerably from those calculated using the SELCON3 program (Table II and Fig. 3), but the predicted sequences of the denatured structures suggest that most of the  $\beta$ -strands in the native state are changed into  $\alpha$ -helices in the TFE and MeOH solutions, and that the two alcohols induce similar structures.

$\alpha$ -Chymotrypsinogen—CGN is a  $\beta$ -protein comprising 7.4%  $\alpha$ -helices (two segments) and 32.2%  $\beta$ -strands (14 segments) with five disulfide bonds. These compositions are almost identical in the A-state [Table II and Fig. 2(f)], which is consistent with CGN being stable over the pH range from 1 to 10.<sup>9</sup> The  $\alpha$ -helix content increases to 63.7% (12 segments) and 40.2% (10 segments) in the TFE and MeOH solutions, respectively, whereas  $\beta$ -strands decrease to 5.1% (three segments) and 14.3% (seven segments). These results suggest that the denatured CGN consists of several long  $\alpha$ -helices and short  $\beta$ -strands connected by coil regions. The secondary-structure sequences [Fig. 3(c)] predict that about half of  $\beta$ -strands in the native state change into  $\alpha$ -helices, and two  $\alpha$ -helices (residues 165–172 and 235–244) are preserved or extended in the TFE and MeOH solutions.

#### Effects of disulfide bonds on alcohol-denatured structures

As indicated in Table II and Figure 2, the helix-forming abilities in TFE and MeOH vary with the type of proteins, which are generally classified into  $\alpha$ -,  $\beta$ -, ( $\alpha + \beta$ )-,  $\alpha/\beta$ -, and disordered groups. However, the small number of proteins investigated in this study makes it difficult to deduce what type of protein is susceptible to alcohol denaturation because the structure of a protein is stabilized by many factors, including electrostatic, hydrophilic, and hydrophobic interactions, and disulfide bonds. Among these factors, the disulfide bonds would play an important role in helix formation by alcohols because the chain flexibility should affect the stability and average length of helix structures. In fact, the secondary structures of disulfide variants of lysozyme are more effectively stabilized through conformational entropy forces as the number of disulfide bonds increases and as they are formed over larger distances in the primary structure.<sup>36</sup> Therefore, to confirm whether the disulfide bonds inhibit or enhance helix formation during alcohol denaturation, we examined the correlation of the helix-forming abilities in TFE and MeOH with the disulfide-bond density of six proteins, defined as the number of disulfide bonds per 100 residues for each protein.

Figure 4(a) plots the increment in the helix content induced by TFE and MeOH relative to the control state

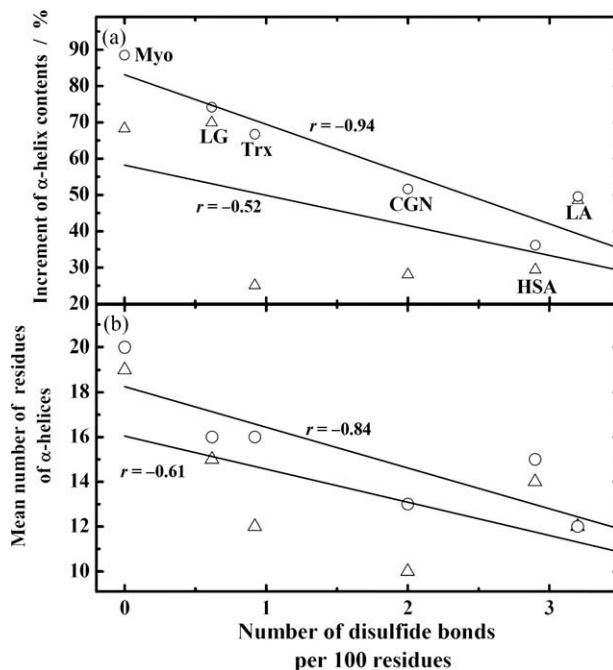


**Figure 4**

Plots of the helix increment (a) and the mean number of residues of  $\alpha$ -helices (b) against the disulfide-bond density of six denatured proteins in 50% TFE (circles) and 70% MeOH (triangles). Solid lines indicate least-squares linear regressions with the correlation coefficient ( $r$ ).

(pH 2) as a function of disulfide-bond density. Evidently, the helix-content increment decreases with increasing disulfide-bond density, with the extent being stronger for TFE (correlation coefficient,  $r = -0.94$ ) than for MeOH ( $r = -0.52$ ). This indicates that the disulfide bonds suppress helix formation by alcohol. To further examine the effects of disulfide bonds on the average length of a helix, the mean number of residues per  $\alpha$ -helix involved in the six alcohol-denatured proteins are plotted against the disulfide-bond density in Figure 4(b), for which the mean numbers of residues per  $\alpha$ -helix of Mb, HSA, LA, Trx, LG, and CGN were calculated from the contents and numbers of helix segments in Table II to be 20, 15, 12, 16, 16, and 13, respectively, in 50% TFE and to be 19, 14, 12, 12, 15, and 10 in 70% MeOH. The negative slopes suggest that the disulfide bonds disturb the persistent helix formation, with the extent being stronger for TFE ( $r = -0.84$ ) than for MeOH ( $r = -0.61$ ). Thus, disulfide bonds inhibit alcohol-induced helix formation. Although it was beyond the scope of this study to consider the effect of each disulfide bond on the formation of helix and strand structures, 46 of the 56 total cysteine residues participating in the disulfide bonds are located on the helix segments in the predicted sequences of six TFE-denatured proteins (Fig. 3 and Supporting Information Fig. S1), with some being located at the C- or N-terminal of helix segments. This constitutes evidence that

disulfide bonds do not introduce a kink into formed helices, although they inhibit helix formation due to the reduced chain flexibility.

A notable finding is that small amounts of  $\beta$ -strands (0.6–14.3%) are produced in the TFE-denatured CGN and in the MeOH-denatured Mb, LA, Trx, LG, and CGN (Table II and Fig. 2). However, there was no significant correlation ( $r = -0.06$ ) between the mean segment length of  $\beta$ -strands and the disulfide-bond density (data not shown), which implies that the chain flexibility does not significantly affect the formation of  $\beta$ -strands by alcohols and hence that most of the produced  $\beta$ -strands would not form rigid  $\beta$ -sheets.

### Generalized features of alcohol-denatured structures

This VUVCD study has revealed some new characteristics of the secondary structures of six proteins denatured by TFE and MeOH. In these analyses,  $\alpha$ -helices,  $\beta$ -strands, and turns were assigned with hydrogen bonds between peptide groups (DSSP program); the contents and numbers of secondary-structure segments were estimated using the SELCON3 program combined with the VUVCD spectra, and their sequences were predicted by the VUVCD-NN method based on the parameters for the native proteins. Because the proteins and alcohols used encompass a wide range of structural characteristics and helix-inducing abilities, respectively, within these analytical limitations we can conclude the following general features for the structures of alcohol-denatured proteins: (1) long  $\alpha$ -helices are dominant, (2) there are very few  $\beta$ -strands, (3) turns are almost unchanged, (4) there are very few PPII structures, and (5) disulfide bonds inhibit helix formation. It should be emphasized that the alcohol-denatured proteins contain many more and longer  $\alpha$ -helices than the native proteins, although  $\alpha$ -helices are greatly disrupted in other types of denaturation<sup>14</sup> except for denaturation by sodium dodecyl sulfate.<sup>52</sup>

The presence of significant correlations between the constituent elements may be useful for understanding the alcohol-denaturation mechanism. Figure 5 plots the contents of  $\beta$ -strands, turns, and unordered structures against the  $\alpha$ -helix contents for all the six proteins denatured by TFE and MeOH. The figure provides evidence of a strong correlation between these secondary-structure contents, suggesting that the newly formed  $\alpha$ -helices are transformed dominantly from  $\beta$ -strands and unordered structures ( $r = -0.93$  and  $-0.94$ , respectively). The weaker correlation for turns ( $r = -0.60$ ) might be due to a reduced transformation of turns into  $\alpha$ -helices because the hydrogen bonds between amide groups are generally promoted by adding alcohols, which stabilizes the  $\beta$ -turn and  $\beta$ -hairpin structures as well as the helical structures.<sup>46,53</sup> It is of interest that both  $\beta$ -strands and unordered structures are transformed into  $\alpha$ -helices in

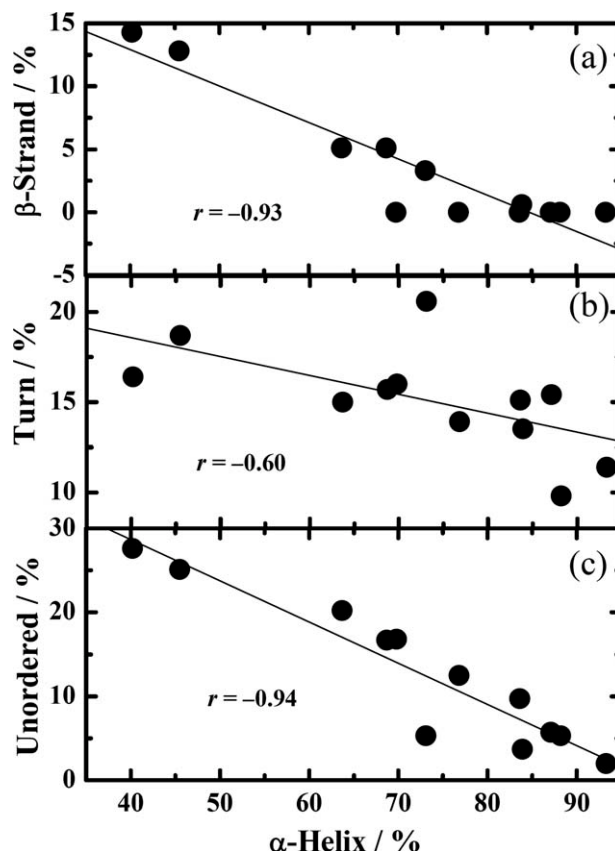


**Figure 5**

Plots of the  $\beta$ -strand (a), turn (b), and unordered-structure (c) contents against  $\alpha$ -helix content for TFE- and MeOH-denatured Mb, HSA, LA, Trx, LG, and CGN.

the alcohol solutions (with a strong correlation), despite it being expected that the correlation should be as weak as for turns if the  $\beta$ -strands form hydrogen bonds with each other. This strong correlation might be due to most of the  $\beta$ -strands induced by alcohols not existing as  $\beta$ -sheets, but rather as several extended peptide segments with the dihedral angles of  $\beta$ -strands, which are abundant in the cold- and heat-denatured states, and the A-state.<sup>14</sup> Such extended  $\beta$ -strands as well as unordered structures could easily be transformed into  $\alpha$ -helices in the alcohol solutions. As evident in Table II, the PPII content is negligible in 50% TFE and 70% MeOH, although a large amount of PPII is formed during other types of denaturation,<sup>14</sup> suggesting that most of the PPII regions are easily transformed into  $\alpha$ -helices in the alcohol solutions because PPII is a non-hydrogen-bonded helix. On the basis of these results, we propose that alcohol-denatured proteins constitute an ensemble of long  $\alpha$ -helices, distorted or extended  $\beta$ -strands, turns, and unordered structures, whose populations and positions depend on the types of alcohols (i.e., the denaturing conditions) and proteins. Alcohol denaturation differs signif-

icantly from other types of denaturation<sup>14</sup> in terms of the contents of  $\alpha$ -helices,  $\beta$ -strands, and PPII structures.

This study has demonstrated that VUVCD spectroscopy can reveal new and important characteristics of the structures of alcohol-denatured proteins. VUVCD spectroscopy combined with theoretical methods (NN algorithms, modeling, and molecular dynamics) would be useful for predicting the content, number of segment, sequence, and spatial orientation of the secondary structures of nonnative (misfolded, membrane-induced, and natively unfolded) proteins, which are closely related to conformation diseases such as amyloid fibril formation and the efficacies of drug delivery systems.

## REFERENCES

- Privalov PL. Cold denaturation of proteins. *Crit Rev Biochem Mol Biol* 1990;25:281–305.
- Dill KA, Shortle D. Denatured states of proteins. *Annu Rev Biochem* 1991;60:795–825.
- Silva JL, Weber G. Pressure stability of proteins. *Annu Rev Phys Chem* 1993;44:89–113.
- Alexandrescu AT, Ng YL, Dobson CM. Characterization of a trifluoroethanol-induced partially folded state of  $\alpha$ -lactalbumin. *J Mol Biol* 1994;235:587–599.
- Lai Z, Colón W, Kelly JW. The acid-mediated denaturation pathway of transthyretin yields a conformational intermediate that can self-assemble into amyloid. *Biochemistry* 1996;35:6470–6482.
- Lu H, Buck M, Radford SE, Dobson CM. Acceleration of the folding of hen lysozyme by trifluoroethanol. *J Mol Biol* 1997;265:112–117.
- Buck M, Radford SE, Dobson CM. A partially folded state of hen egg white lysozyme in trifluoroethanol: structural characterization and implications for protein folding. *Biochemistry* 1993;32:669–678.
- Babu KR, Douglas DJ. Methanol-induced conformations of myoglobin at pH 4.0. *Biochemistry* 2000;39:14702–14710.
- Khan F, Khan RH, Muzammil S. Alcohol-induced versus anion-induced states of  $\alpha$ -chymotrypsinogen A at low pH. *Biochim Biophys Acta* 2000;1481:229–336.
- Xu Q, Keiderling TA. Trifluoroethanol-induced unfolding of concanavalin A: equilibrium and time-resolved optical spectroscopic studies. *Biochemistry* 2005;44:7976–7987.
- Wang Y, Shortle D. The equilibrium folding pathway of staphylococcal nuclease: identification of the most stable chain–chain interactions by NMR and CD spectroscopy. *Biochemistry* 1995;34:15895–15905.
- From NB, Bowler BE. Urea denaturation of staphylococcal nuclease monitored by Fourier transform infrared spectroscopy. *Biochemistry* 1998;37:1623–1631.
- Whittington SJ, Chellgren BW, Hermann VM, Creamer TP. Urea promotes polyproline II helix formation: implications for protein denatured states. *Biochemistry* 2005;44:6269–6275.
- Matsuo K, Sakurada Y, Yonehara R, Kataoka M, Gekko K. Secondary-structure analysis of denatured proteins by vacuum-ultraviolet circular dichroism spectroscopy. *Biophys J* 2007;92:4088–4096.
- Kanjilal S, Taulier N, Le Huérou JY, Gindre M, Urbach W, Waks M. Ultrasonic studies of alcohol-induced transconformation in beta-lactoglobulin: the intermediate state. *Biophys J* 2003;85:3928–3934.
- Ptitsyn OB. The molten globule state in Protein Folding. In: Creighton, TE, editor. *Protein folding*. New York: Freeman; 1992. pp 243–300.
- Nishii I, Kataoka M, Tokunaga F, Goto Y. Cold denaturation of the molten globule states of apomyoglobin and a profile for protein folding. *Biochemistry* 1994;33:4903–4909.
- Harding MM, Williams DH, Woolfson DN. Characterization of a partially denatured state of a protein by two-dimensional NMR: reduction of the hydrophobic interactions in ubiquitin. *Biochemistry* 1991;30:3120–3128.
- Dong A, Matsuura J, Manning MC, Carpenter JF. Intermolecular  $\beta$ -sheet results from trifluoroethanol-induced nonnative  $\alpha$ -helical structure in  $\beta$ -sheet predominant proteins: infrared and circular dichroism spectroscopic study. *Arch Biochem Biophys* 1998;355:275–281.
- Bhakuni V. Alcohol-induced molten globule intermediates of proteins: are they real folding intermediates or off pathway products? *Arch Biochem Biophys* 1998;357:274–284.
- Shiraki K, Nishikawa K, Goto Y. Trifluoroethanol-induced stabilization of the  $\alpha$ -helical structure of  $\beta$ -lactoglobulin: implication for non-hierarchical protein folding. *J Mol Biol* 1995;245:180–194.
- Hirota N, Mizuno K, Goto Y. Cooperative  $\alpha$ -helix formation of  $\beta$ -lactoglobulin and melittin induced by hexafluoroisopropanol. *Protein Sci* 1997;6:416–421.
- Kuwata K, Hoshino M, Era S, Batt CA, Goto Y.  $\alpha \rightarrow \beta$  transition of  $\beta$ -lactoglobulin as evidenced by heteronuclear NMR. *J Mol Biol* 1998;283:731–739.
- Kamatari YO, Ohji S, Konno T, Seki Y, Soda K, Kataoka M, Akasaka K. The compact and expanded denatured conformations of apomyoglobin in the methanol–water solvent. *Protein Sci* 1999;8:873–882.
- Kamatari YO, Konno T, Kataoka M, Akasaka K. The methanol-induced transition and the expanded helical conformation in hen lysozyme. *Protein Sci* 1998;7:681–688.
- Kabsch W, Sander C. Dictionary of protein secondary structure: pattern recognition of hydrogen-bonded and geometrical features. *Biopolymers* 1983;22:2577–2637.
- King SM, Johnson WC. Assigning secondary structure from protein coordinate data. *Proteins* 1999;35:313–320.
- Sreerama N, Woody RW. Estimation of protein secondary structure from circular dichroism spectra: comparison of CONTIN, SELCON, and CDSSTR methods with an expanded reference set. *Anal Biochem* 2000;287:252–260.
- Sreerama N, Venyaminov SY, Woody RW. Estimation of the number of  $\alpha$ -helical and  $\beta$ -strand segments in proteins using circular dichroism spectroscopy. *Protein Sci* 1999;8:370–380.
- Toumadje A, Alcorn SW, Johnson WC Jr. Extending CD spectra of proteins to 168 nm improves the analysis for secondary structure. *Anal Biochem* 1992;200:321–331.
- Jones GR, Clarke DT. Applications of extended ultra-violet circular dichroism spectroscopy in biology and medicine. *Faraday Discuss* 2004;126:223–236.
- Wallace BA, Wien F, Miles AJ, Lees JG, Hoffmann SV, Evans P, Wistow GJ, Slingsby C. Biomedical applications of synchrotron radiation circular dichroism spectroscopy: identification of mutant proteins associated with disease and development of a reference database for fold motifs. *Faraday Discuss* 2004;126:237–243.
- Matsuo K, Yonehara R, Gekko K. Secondary-structure analysis of proteins by vacuum-ultraviolet circular dichroism spectroscopy. *J Biochem* 2004;135:405–411.
- Matsuo K, Yonehara R, Gekko K. Improved estimation of the secondary structures of proteins by vacuum-ultraviolet circular dichroism spectroscopy. *J Biochem* 2005;138:79–88.
- Matsuo K, Watanabe H, Gekko K. Improved sequence-based prediction of protein secondary structures by combining vacuum-ultraviolet circular dichroism spectroscopy with neural network. *Proteins* 2008;73:104–112.
- Matsuo K, Watanabe H, Tate S, Tachibana H, Gekko K. Comprehensive secondary-structure analysis of disulfide variants of lysozyme by synchrotron-radiation vacuum-ultraviolet circular dichroism. *Proteins* 2009;77:191–201.
- Matsuo K, Namatame H, Taniguchi M, Gekko K. Membrane-induced conformational change of  $\alpha_1$ -acid glycoprotein characterized by vacuum-ultraviolet circular dichroism spectroscopy. *Biochemistry* 2009;48:9103–9111.

38. Kumar Y, Muzammil S, Tayyab S. Influence of fluoro, chloro and alkyl alcohols on the folding pathway of human serum albumin. *J Biochem* 2005;138:335–341.
39. Richardson JM III, Lemaire SD, Jacquot JP, Makhatadze GI. Difference in the mechanisms of the cold and heat induced unfolding of thioredoxin h from *Chlamydomonas reinhardtii*: spectroscopic and calorimetric studies. *Biochemistry* 2000;39:11154–11162.
40. Ojima N, Sakai K, Matsuo K, Matsui T, Fukazawa T, Namatame H, Taniguchi M, Gekko K. Vacuum-ultraviolet circular dichroism spectrophotometer using synchrotron radiation: optical system and on-line performance. *Chem Lett* 2001;30:522–523.
41. Matsuo K, Sakai K, Matsushima Y, Fukuyama T, Gekko K. Optical cell with a temperature-control unit for a vacuum-ultraviolet circular dichroism spectrophotometer. *Anal Sci* 2003;19:129–132.
42. Jones DT. Protein secondary structure prediction based on position-specific scoring matrices. *J Mol Biol* 1999;292:195–202.
43. Bernstein FC, Koetzle TF, Williams GJB, Meyer EF Jr, Brice MD, Rodgers JR, Kennard O, Shimanouchi T, Tasumi M. The Protein Data Bank: a computer-based archival file for macromolecular structures. *J Mol Biol* 1977;112:535–542.
44. Zell A, Mamier G, Vogt M, Mache N, Hubner R, Doring S, Herrmann KW, Soyez T, Schmalzl M, Sommer T, Hatzigeorgiou A, Posselt D, Schreiner T, Kett B, Clemente G, Wieland J. Stuttgart neural network simulator, Version 4.2. Stuttgart, Germany: University of Stuttgart; 1995. <http://www.ra.cs.uni-tuebingen.de/downloads/SNNS>.
45. Kumar Y, Tayyab S, Muzammil S. Molten-globule like partially folded states of human serum albumin induced by fluoro and alkyl alcohols at low pH. *Arch Biochem Biophys* 2004;426:3–10.
46. Gast K, Zirwer D, Müller-Frohne M, Damaschun G. Trifluoroethanol-induced conformational transitions of proteins: insights gained from the differences between  $\alpha$ -lactalbumin and ribonuclease A. *Protein Sci* 1999;8:625–634.
47. Pancoska P, Janota V, Keiderling TA. Novel matrix descriptor for secondary structure segments in proteins: demonstration of predictability from circular dichroism spectra. *Anal Biochem* 1999;267:72–83.
48. Yao J, Chung J, Eliezer D, Wright PE, Dyson HJ. NMR structural and dynamic characterization of the acid-unfolded state of apomyoglobin provides insights into the early events in protein folding. *Biochemistry* 2001;40:3561–3571.
49. Sugio S, Kashima A, Mochizuki S, Noda M, Kobayashi K. Crystal structure of human serum albumin at 2.5 Å resolution. *Protein Eng* 1999;12:439–446.
50. Reutimann H, Straub B, Luisi PL, Holmgren A. A conformational study of thioredoxin and its tryptic fragments. *J Biol Chem* 1981;256:6796–6803.
51. Kuwata K, Hoshino M, Forge V, Era S, Batt CA, Goto Y. Solution structure and dynamics of bovine  $\beta$ -lactoglobulin A. *Protein Sci* 1999;8:2541–2545.
52. Xu Q, Keiderling TA. Effect of sodium dodecyl sulfate on folding and thermal stability of acid-denatured cytochrome c: a spectroscopic approach. *Protein Sci* 2004;13:2949–2959.
53. Thomas PD, Dill KA. Local and nonlocal interactions in proteins and mechanisms of alcohol denaturation. *Protein Sci* 1993;2:2050–2065.